Internal deformation of the subducted Nazca slab inferred from seismic anisotropy

Caroline M. Eakin[1,2]*, Maureen D. Long[1], Alissa Scire[3], Susan L. Beck[3], Lara S. Wagner[4], George Zandt[3] and Hernando Tavera[5]

Within oceanic lithosphere a fossilized fabric is often preserved originating from the time of plate formation. Such fabric is thought to form at the mid-ocean ridge when olivine crystals align with the direction of plate spreading[1,2]. It is unclear, however, whether this fossil fabric is preserved within slabs during subduction or overprinted by subduction-induced deformation. The alignment of olivine crystals, such as within fossil fabrics, can generate anisotropy that is sensed by passing seismic waves. Seismic anisotropy is therefore a useful tool for investigating the dynamics of subduction zones, but it has so far proved difficult to observe the anisotropic properties of the subducted slab itself. Here we analyse seismic anisotropy in the subducted Nazca slab beneath Peru and find that the fast direction of seismic wave propagation aligns with the contours of the slab. We use numerical modelling to simulate the olivine fabric created at the mid-ocean ridge, but find it is inconsistent with our observations of seismic anisotropy in the subducted Nazca slab. Instead we find that an orientation of the olivine crystal fast axes aligned parallel to the strike of the slab provides the best fit, consistent with along-strike extension induced by flattening of the slab during subduction (A. Kumar *et al.*, manuscript in preparation). We conclude that the fossil fabric has been overprinted during subduction and that the Nazca slab must therefore be sufficiently weak to undergo internal deformation.

It has long been suggested that the process of seafloor spreading at mid-ocean ridges (MOR) induces a lattice preferred orientation (LPO) of olivine in the underlying mantle that is subsequently 'frozen-in' to the oceanic plate during its formation[1,2]. For A-type olivine LPO fabrics, typical of dry oceanic lithosphere, the fast *a* axes of olivine tend to align with the plate spreading direction, resulting in a fossilized crystallographic fabric in the oceanic plate[3,4]. Such fossilized fabric will manifest itself as seismic anisotropy, the phenomenon by which seismic wave velocity is directionally dependent. Observations from surface-wave-derived azimuthal anisotropy[5–7], shear wave splitting[8,9], and refracted P-wave (Pn) velocities[10] all indicate that seismic anisotropy within the oceanic lithosphere is consistent with the concept of fossil spreading.

In subduction zones, where oceanic plates descend into the mantle, it is unclear whether this fossil spreading fabric is preserved within the slab to depth, or if the anisotropic signal is overprinted by subsequent subduction-associated deformation. Observations that directly constrain intra-slab anisotropy are limited in number[11,12], and completely absent for the deep portions of slabs (below 200 km). An alternative model for slab anisotropy invokes vertically aligned,

hydrated faults in the upper portion of the slab that result from bending stresses at the outer rise. This phenomenon could result in seismically inferred fast directions that are parallel to the trench, owing to a combined SPO (shape preferred orientation) and LPO effect of the serpentinized faults[13], which is consistent with some P-wave and Rayleigh wave observations[14–16] (down to a maximum depth of 200 km).

The most direct observations of seismic anisotropy usually come from shear wave splitting, whereby the orientation of the fast polarized shear wave (ϕ) and the delay time (δt) between the fast and the slow polarized waves are measured. For most shear wave splitting studies targeting subduction zones, anisotropy within the slab itself is typically disregarded because the relative path length through the slab is small compared to the rest of the upper mantle. For the Nazca slab beneath Peru, however, the unique flat-slab geometry, with a transition from a shallow to steeply dipping slab ~500 km inboard from the trench (Fig. 1), allowed us to make splitting measurements on the seismic S phases with relatively long path lengths through the slab (see Methods), which would normally be difficult to observe. Using data from the PULSE and PeruSE arrays, we obtained 16 splitting measurements (out of 36 suitable arrivals) for deep local S phases (Fig. 2a), with the majority of fast directions oriented approximately N–S (mean ϕ: −6.3), and exhibiting substantial delay times (mean δt: 1.3 s). In the same vicinity as the local S results (for example, area encircled by dashed line in Fig. 2a), source-side measurements on down-going S phases measured at distant stations show very similar splitting characteristics (mean ϕ: −1.2°, mean δt: 1.6 s, number of measurements: 9), indicating that the two types of phases sample may the same anisotropic source region.

Several lines of argument suggest that this main anisotropic source is within the subducting Nazca slab. First, when the ray paths are plotted in three dimensions (see Supplementary Information) and compared against the slab outline from regional S-wave tomography[17], it is clear that many rays (both local S and source side) have long path lengths through the slab (Fig. 2a, Supplementary Figs 1 and 2 and Supplementary Movie 1). In particular, a cluster of N–S-oriented fast splitting measurements towards the centre of the study area travel through relatively fast (blue) material all the way from the mid-transition zone (555 km) to the mid-upper mantle (<200 km), representing a total path length of over 250 km through the slab (Supplementary Fig. 1). We also note that this N–S ϕ orientation roughly correlates with the N–S strike of the subducting Nazca Plate. Outside of the slab, for measurements that sample mainly sub-slab mantle, the fast directions are generally
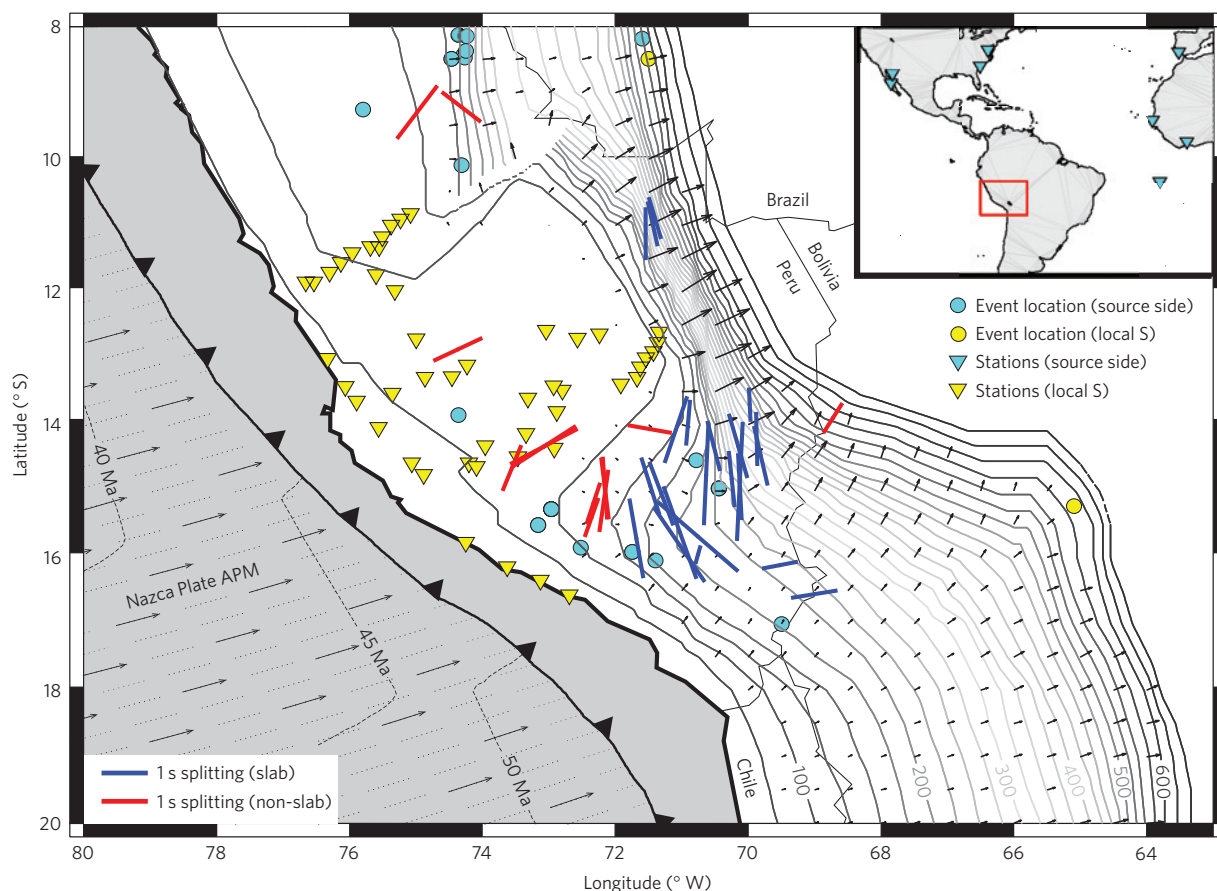
Figure 1 | Tectonic setting of southern Peru, showing the distribution of stations and events, and comparing the splitting results with the slab geometry. Slab contours are derived from the regional tomography model and represent the midpoint of the slab at that depth[17]. Black arrows illustrate the slab dip vectors—that is, the gradient of the contours. Splitting results (blue and red bars) are plotted at their pierce point at 300 km depth. The orientation of the bar represents φ, and its length is scaled by δt. Absolute plate motions (APM; ref. 28) and seafloor age contours[29] are shown for the Nazca Plate.

trench perpendicular (ENE–WSW), most likely reflecting trench normal mantle flow beneath the flat slab[18]. This flow direction is opposite to that previously inferred by less direct SKS splitting methods[19], and is discussed in detail in our earlier work[18,20].

Another line of evidence for distinct anisotropy within the slab itself comes from the fact that the most of the local S phases arrive ∼5–10 s earlier than predicted by our reference velocity model (Fig. 2b). The S-waves must therefore be travelling through relatively fast material with a velocity anomaly of the order of +3.5% (±1.5%) to account for the travel time difference. The magnitude of this required velocity anomaly is comparable to the strength of the velocity anomaly present in the slab (Fig. 2a), as estimated from the tomographic inversion[17].

Yet another telling observation is the fact that the two slowest local S phases, which arrive close to the expected arrival time (see FM05 and FS12 in Fig. 2b), exhibit contrasting fast directions (WNW–ESE and NE–SW; green lines in Fig. 2a) in comparison with the remainder of the local S data set (approximately N–S). When compared against the tomography, the ray paths associated with these two measurements mostly sample outside the slab, especially in the 200–400 km depth range (Fig. 2a and Supplementary Fig. 1).

On the basis of the evidence outlined above, we have a group of 23 splitting measurements (14 from local S and 9 from source-side teleseismic S) that we infer to reflect intra-slab anisotropy (blue bars in Fig. 1). The average splitting parameters of this sub-set are −3.4° for φ (s.d.: 27°) and 1.4 s for δt (s.d.: 0.6 s). On the basis of the splitting pattern and the slab geometry, as well as other criteria (see Supplementary Information), we infer that the main source of

anisotropy seems to lie between 200 and 400 km depth within the slab. Considering this path length of ∼200 km through anisotropic material then this would imply an anisotropic strength of ∼3–4%, consistent with observations from other subducted slabs[21,22]. When compared to the slab morphology (Fig. 1), the fast-axis orientation of these slab splitting results generally seem to be sub-parallel to the slab contours, with over three-quarters of measurements oriented within 33° of the slab strike (Supplementary Fig. 3). Because the slab morphology can change abruptly, it is possible that several geometries are sampled along any single ray path, which may account for some of the scatter in the results. In general, however, our inference of φ values aligned with the slab strike contrasts with observations of azimuthal anisotropy within the Nazca Plate before it subducts beneath South America[5–7]. These show fast axes sub-parallel to the palaeo-spreading direction (roughly E–W), consistent with fossilized A-type (or similar) olivine fabric.

To quantitatively test the hypothesis that the slab preserves the fossil fabric to depth, we carry out a series of forward models based on likely elastic tensors for the upper mantle (see Methods and Supplementary Information). For all fabric types considered (olivine A-, B-, C-, and E-type, plus a natural peridotite), the mean angle of misfit between the modelled fast directions and those measured by shear wave splitting (Supplementary Fig. 4) is far greater than the standard observational errors (<20°). This demonstrates that none of the fabric types considered provides a good fit to the data under the assumption of frozen-in anisotropy, indicating that the fabric frozen within the Nazca Plate must have been overprinted or otherwise modified during subduction.
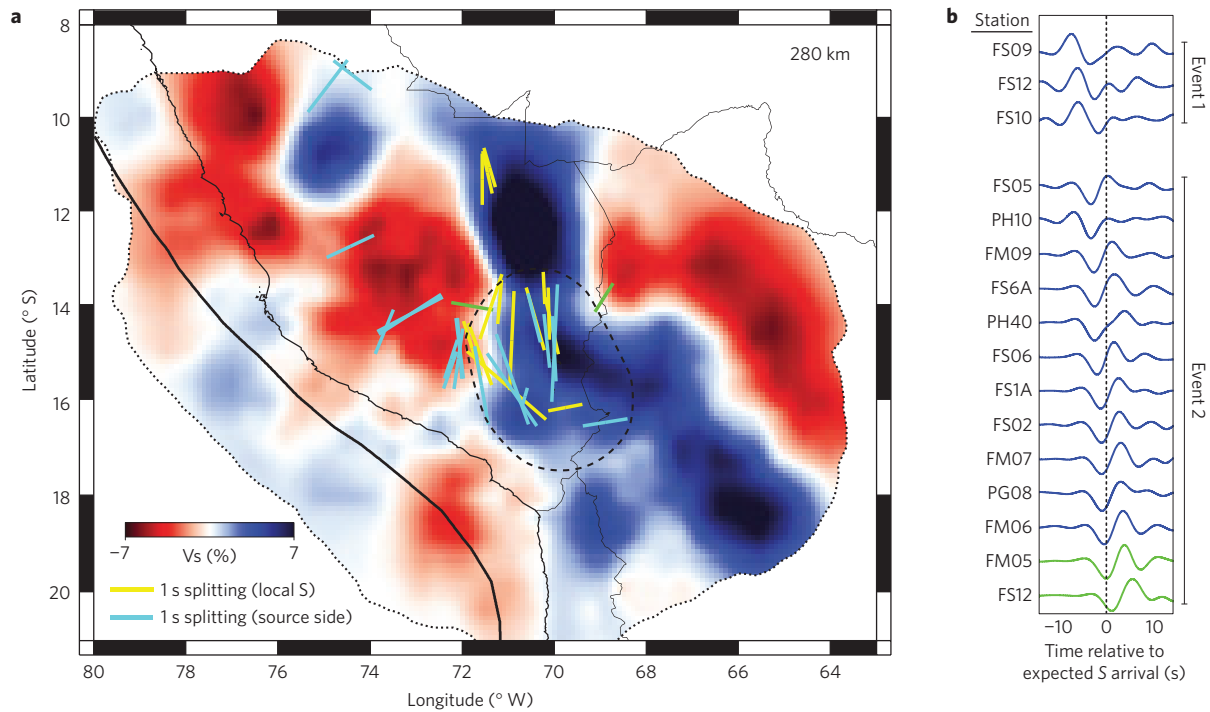
Figure 2 | Comparison of the regional splitting pattern with seismic signatures of the subducting slab. a, Shear wave splitting results overlain on S-wave tomography[17]. Splitting measurements are the same as Fig. 1. Within the area enclosed by the dashed circle, which overlies the slab (linear dark blue feature), the source-side and local S splits show similar characteristics. Two local S splits (shown in green) that lie outside the slab show contrasting orientations. **b,** Record section of local S phases for which splitting was measured. Records are grouped by event and then sorted by arrival time relative to the reference velocity model (Supplementary Table 1). The normalized horizontal component in the direction of initial polarization is plotted. All seismograms are bandpass filtered from 0.03 to 0.15 Hz. The two slowest phase arrivals correspond to the green results in sub-figure (**a**).
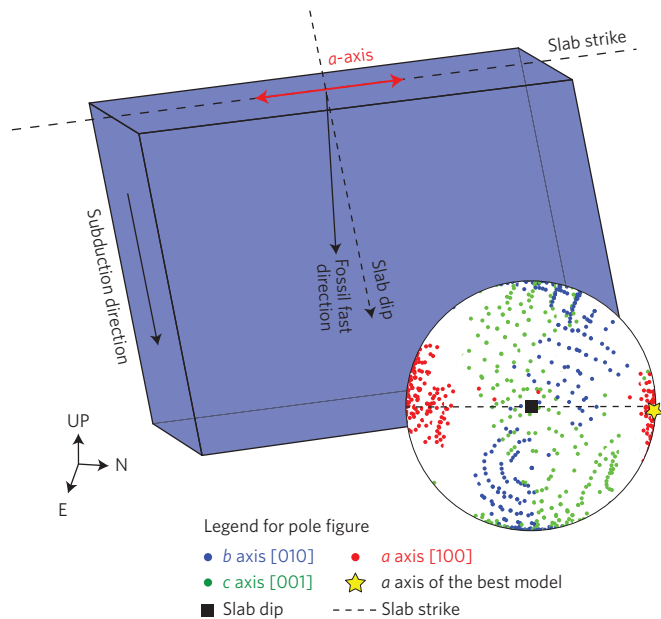

Figure 3 | Summary of the modelling results illustrating the orientation of olivine that would best reproduce the slab splitting fast directions. The pole figure (upper hemisphere plotted, looking from above) shows the crystal preferred orientation (CPO) of the main crystal axes (*a*, *b* and *c*) that would be required by A-type olivine in the upper mantle for the top 1% of models. The similarly slow *b* and *c* axes (blue and green dots) are randomly oriented in the symmetry plane, but the fast *a* axes (red dots) tend to cluster parallel with the slab strike. This favourable *a* axis orientation is illustrated on the blue cartoon slab.

Taking a different approach, we also select the olivine fabric type most likely for dry oceanic lithosphere (A-type)[4] and perform a grid search over all possible three-dimensional rotations to find the orientation (relative to the slab strike and dip) which best predicts our slab splitting results (see Supplementary Information). Analysing the top 1% of best-fitting models (Supplementary Fig. 5) reveals a strong clustering of the olivine *a*-axes pointing towards the slab strike (red dots, Fig. 3). This best-fit orientation also predicts >3% anisotropy for our ray paths, which can easily reproduce our delay times with reasonable path lengths through the slab (~200 km; Supplementary Fig. 6).

An alternative explanation for our measurements could invoke the LPO of wadsleyite within the slab at depths below the olivine-to-wadsleyite transition (~410 km). Forward modelling demonstrates that wadsleyite provides an acceptable fit to the data (Supplementary Fig. 7a), but considering the spatial distribution of splitting patterns indicates that the main source of anisotropy is unlikely to be in the transition zone (see Supplementary Information). A third possibility for intra-slab anisotropy could be from SPO-type mechanisms such as aligned serpentinized faults[13]. Although shallow hydrous phases such as serpentine will become progressively unstable with increasing pressure, a transformation to DHMS (dense hydrous magnesium silicates)[23] could potentially still contribute to our deep anisotropic source (below 200 km). However, this hydrated layer is probably relatively thin, and the predicted faulting geometry is non-optimal for reproducing our splitting observations (Supplementary Information).

On the basis of our observations and models, it seems likely that the LPO within the subducted lithosphere has been modified by deformation in the upper mantle, with the fast axes of olivine rotated ~90° from the fossil spreading direction (approximately down-dip) to be sub-parallel to the slab strike. This implies either along-strike

shear or extension in the slab; either scenario would align the fast axes parallel to the slab strike[4] (the sense of shear is unresolved). Along-strike extension is reasonable given the contorted slab morphology and abrupt bends in the contours (Fig. 1). This scenario is also supported by T-axes (that is, the direction of maximum extension) inferred from earthquake focal mechanisms, which also follow the strike of the Nazca slab where it transitions from flat to steep (A. Kumar *et al.*, manuscript in preparation).

Our inference contrasts with the standard view of slabs as cold, rigid, elastic plates that are strong enough to resist permanent internal deformation and therefore preserve fossil anisotropy to depth. Instead, our results imply that the Nazca slab may deform relatively easily, and may thus be relatively weak. The development of new LPO (and overprinting of previously existing LPO) in particular directly implies plastic deformation in the dislocation creep regime at relatively large strains. In comparison, simple geometrical estimates of the slab bending strain[24], based on the curvature of the slab contours, have an upper range of $\varepsilon = 1.0$–1.4 (see Supplementary Fig. 8).

The view of slab deformation indicated by our observations is consistent with some geodynamical modelling; for example, viscous deformation is required to explain the global geoid pattern[25]. The relative amount of viscous versus elastic deformation within slabs is still debated[26,27], perhaps in part because we lack direct observations of the non-elastic strain. Analysis of intra-slab seismic anisotropy such as that described here may therefore provide important new constraints on the deformation and rheology of subducting slabs as they descend through the mantle. A crucial observational limitation, however, lies in the difficulty of isolating the anisotropic signature of the slab. As we found previously in Peru[18,20], standard SKS splitting analysis may hint at the presence of intra-slab anisotropy, but cannot constrain it, given that path lengths through the slab are relatively short. It remains to be investigated, therefore, whether other subduction zones exhibit similar modification of the fossilized slab fabric at depth, or if this is unique to the relatively young, warm, and distorted Nazca slab.

Methods

Methods and any associated references are available in the [online version of the paper](#).

References

1. Francis, T. Generation of seismic anisotropy in the upper mantle along the mid-oceanic ridges. *Nature* **221,** 162–165 (1969).
2. Hess, H. Seismic anisotropy of the uppermost mantle under oceans. *Nature* **203,** 629–631 (1964).
3. Zhang, S. & Karato, S. Lattice preferred orientation of olivine aggregates deformed in simple shear. *Nature* **375,** 774–777 (1995).
4. Karato, S. *Deformation of Earth Materials. An Introduction to the Rheology of Solid Earth* (Cambridge Univ. Press, 2008).
5. Maggi, A., Debayle, E., Priestley, K. & Barruol, G. Azimuthal anisotropy of the Pacific region. *Earth Planet. Sci. Lett.* **250,** 53–71 (2006).
6. Debayle, E. & Ricard, Y. Seismic observations of large-scale deformation at the bottom of fast-moving plates. *Earth Planet. Sci. Lett.* **376,** 165–177 (2013).
7. Beghein, C., Yuan, K., Schmerr, N. & Xing, Z. Changes in seismic anisotropy shed light on the nature of the Gutenberg discontinuity. *Science* **343,** 1237–1240 (2014).
8. Wolfe, C. & Silver, P. Seismic anisotropy of oceanic upper mantle: Shear wave splitting methodologies and observations. *J. Geophys. Res.* **103,** 749–771 (1998).
9. Harmon, N., Forsyth, D. W., Fischer, K. M. & Webb, S. C. Variations in shear-wave splitting in young Pacific seafloor. *Geophys. Res. Lett.* **31,** L15609 (2004).
10. Gaherty, J. B., Lizarralde, D., Collins, J. A., Hirth, G. & Kim, S. Mantle deformation during slow seafloor spreading constrained by observations of seismic anisotropy in the western Atlantic. *Earth Planet. Sci. Lett.* **228,** 255–265 (2004).
11. Audet, P. Seismic anisotropy of subducting oceanic uppermost mantle from fossil spreading. *Geophys. Res. Lett.* **40,** 173–177 (2013).
12. Song, T.-R. A. & Kim, Y. Anisotropic uppermost mantle in young subducted slab underplating Central Mexico. *Nature Geosci.* **5,** 55–59 (2012).
13. Faccenda, M., Burlini, L., Gerya, T. V. & Mainprice, D. Fault-induced seismic anisotropy by hydration in subducting oceanic plates. *Nature* **455,** 1097–1100 (2008).
14. Eberhart-Phillips, D. & Reyners, M. Three-dimensional distribution of seismic anisotropy in the Hikurangi subduction zone beneath the central North Island, New Zealand. *J. Geophys. Res.* **114,** B06301 (2009).
15. Wagner, L., Fouch, M., James, D. & Long, M. The role of hydrous phases in the formation of trench parallel anisotropy: Evidence from Rayleigh waves in Cascadia. *Geophys. Res. Lett.* **40,** 1–5 (2013).
16. Yu, D. & Wang, L. P-wave anisotropy tomography of central Japan: Insight into subduction dynamics. *Tectonophysics* **592,** 14–30 (2013).
17. Scire, A. *et al.* Imaging the transition from flat to normal subduction: variations in the structure of the Nazca slab and upper mantle under southern Peru and northwestern Bolivia. *Geophys. J. Int.* (in the press).
18. Eakin, C. M. & Long, M. D. Complex anisotropy beneath the Peruvian flat slab from frequency-dependent, multiple-phase shear wave splitting analysis. *J. Geophys. Res.* **118,** 4794–4813 (2013).
19. Russo, R. & Silver, P. Trench-parallel flow beneath the Nazca plate from seismic anisotropy. *Science* **263,** 1105–1111 (1994).
20. Eakin, C. M., Long, M. D., Wagner, L. S., Beck, S. L. & Tavera, H. Upper mantle anisotropy beneath Peru from SKS splitting: Constraints on flat slab dynamics and interaction with the Nazca Ridge. *Earth Planet. Sci. Lett.* **412,** 152–162 (2015).
21. Matchem, I., Savage, M. K. & Gledhill, K. R. Distribution of seismic anisotropy in the subduction zone beneath the Wellington region, New Zealand. *Geophys. J. Int.* **140,** 1–10 (2000).
22. Hiramatsu, Y., Ando, M. & Ishikawa, Y. ScS wave splitting of deep earthquakes around Japan. *Geophys. J. Int.* **128,** 409–424 (1997).
23. Faccenda, M. Water in the slab: A trilogy. *Tectonophysics* **614,** 1–30 (2014).
24. Turcotte, D. L. & Schubert, G. *Geodynamics* (Cambridge Univ. Press, 2002).
25. Hager, B. Subducted slabs and the geoid: Constraints on mantle rheology and flow. *J. Geophys. Res.* **89,** 6003–6015 (1984).
26. Farrington, R. J., Moresi, L.-N. & Capitanio, F. A. The role of viscoelasticity in subducting plates. *Geochem. Geophys. Geosyst.* **15,** 4291–4304 (2014).
27. Fourel, L., Goes, S. & Morra, G. The role of elasticity in slab bending. *Geochem. Geophys. Geosyst.* **15,** 4507–4525 (2014).
28. Gripp, A. E. & Gordon, R. G. Young tracks of hotspots and current plate velocities. *Geophys. J. Int.* **150,** 321–361 (2002).
29. Müller, R., Sdrolias, M., Gaina, C. & Roest, W. Age, spreading rates, and spreading asymmetry of the world's ocean crust. *Geochem. Geophys. Geosyst.* **9,** 18–36 (2008).

Author contributions

C.M.E. conceived the paper topic, made the measurements, and carried out the modelling in collaboration with M.D.L.; A.S. and G.Z. provided the tomographic images and slab contours; M.D.L., S.L.B., L.S.W. and H.T. were principal investigators on the PULSE deployment; C.M.E. and M.D.L. co-wrote the paper with feedback and input from all co-authors.

Additional information

Supplementary information is available in the [online version of the paper](#). Reprints and permissions information is available online at www.nature.com/reprints. Correspondence and requests for materials should be addressed to C.M.E.

Competing financial interests

The authors declare no competing financial interests.

Methods

Shear wave splitting analysis. We investigated shear wave splitting for local S phases originating from deep (>500 km) events at 40 seismic stations of the PULSE (PerU Lithosphere and Slab Experiment) array, along with 8 stations from the PeruSE (Peru Subduction Experiment) network (Fig. 1). Both networks were in operation over a similar ~2.5 year time frame from late 2010 to mid 2013. We searched for deep local events in the Global Centroid-Moment-Tensor (CMT) catalogue[30] yielding S phases that arrived at the stations with incidence angles less than 35°. We found two events that fit this criterion, with moment magnitudes of 5.2 and 6.6, occurring at depths of 533 km and 568 km, respectively (Fig. 1). The small number of suitable events is due to the temporary nature of the deployment and the scarcity of deep earthquakes in this area. Local S splitting analyses on shallower events (40–170 km) are more abundant and reflect anisotropy above the flat slab[31].

Following our previous work[31], we conducted shear wave splitting measurements using the SplitLab software package[32], using the rotation correlation (RC) and eigenvalue (EV) measurement methods for estimating the splitting parameters (ϕ and δt) simultaneously. A variable bandpass filter was applied to all seismograms to improve the signal to noise ratio; the lower cutoff limit of the filter varied from 0.01 to 0.04 Hz and the upper cutoff from 0.1 to 0.3 Hz. Quality control procedures followed previous work[31]; error estimates were typically less than ±12° in ϕ, and ±0.2 s in δt, at the 95% confidence level.

We integrated our deep local S splitting measurements with our previously published source-side splitting data set[18]. The source-side technique uses direct teleseismic S waves originating from local earthquakes in the Nazca slab (event depth range 100–200 km) and measured at distant stations to isolate the contribution from anisotropy beneath the earthquake source, assuming an isotropic lower mantle and applying a correction for upper mantle anisotropy beneath the receiver if needed. Owing to this geometrical set-up, fast directions measured at the station must be reflected across the great circle path (that is, the azimuth) to correct for the down-going versus up-going wave propagation frame of reference. We updated the data set by adding new splitting measurements from station PVAQ, which, as with stations used previously, exhibits negligible splitting of SKS phases[33], indicating an effectively isotropic upper mantle beneath the station. Teleseismic S splitting measurements followed the same procedure as used in our previous work[18].

Forward modelling. We used the Matlab Seismic Anisotropy Toolkit (MSAT; ref. 34) to predict fast splitting directions for a series of elastic tensors that represent different olivine LPO scenarios, along with single-crystal wadsleyite. Each candidate elastic tensor was rotated using the Bunge Euler convention[35] into the candidate orientation. After rotation, we solved the Christoffel equation to predict the orientation of the fast quasi-S wave for the ray propagation direction associated with each ray in the shear wave splitting data set. Fossil spreading scenarios were tested by rotating elastic tensors for various olivine fabric types into an orientation defined by the local slab geometry. The best-fitting A-type olivine fabric orientation was identified by performing a grid search in 10° increments over all possible values for three rotation angles and calculating a mean angular misfit for the entire splitting data set. Further details of the forward modelling methods and results can be found in the Supplementary Information.

Data sources. A compilation of all shear wave splitting measurements presented during this study, including station and event information, is provided as an Excel file under the Supplementary Methods section. All the raw seismic data was accessed via the IRIS DMC (Incorporated Research Institutions for Seismology Data Management Center: http://ds.iris.edu/ds/nodes/dmc). Seismic networks from which data were retrieved include the Global Seismograph Network, the United States National Seismic Network, the Global Telemetered Seismograph Network, GEOSCOPE, the NARS Array, the Portuguese National Seismic Network, the PerU Lithosphere and Slab Experiment and the Peru Subduction Experiment. All seismic data is now publicly available.

Code availability. The SplitLab software package[32] was used to make the shear wave splitting measurements. SplitLab is freely accessible here: http://splitting.gm.univ-montp2.fr. Modelling of the anisotropic fabrics was performed using the Matlab Seismic Anisotropy Toolkit (MSAT; ref. 34) which can be downloaded from: http://www1.gly.bris.ac.uk/MSAT.

References

30. Ekström, G., Nettles, M. & Dziewoński, A. M. The Global CMT project 2004–2010: Centroid-moment tensors for 13,017 earthquakes. *Phys. Earth Planet. Inter.* **200–201,** 1–9 (2012).
31. Eakin, C. M. *et al.* Response of the mantle to flat slab evolution: Insights from local S splitting beneath Peru. *Geophys. Res. Lett.* **41,** 3438–3446 (2014).
32. Wüstefeld, A., Bokelmann, G., Zaroli, C. & Barruol, G. SplitLab: A shear-wave splitting environment in Matlab. *Comput. Geosci.* **34,** 515–528 (2008).
33. Lynner, C. & Long, M. D. Sub-slab seismic anisotropy and mantle flow beneath the Caribbean and Scotia subduction zones: Effects of slab morphology and kinematics. *Earth Planet. Sci. Lett.* **361,** 367–378 (2013).
34. Walker, A. M. & Wookey, J. MSAT—A new toolkit for the analysis of elastic and seismic anisotropy. *Comput. Geosci.* **49,** 81–90 (2012).
35. Bunge, H. J. in *Preferred Orientation in Deformed Metal and Rocks: An Introduction to Modern Texture Analysis* (ed. Wenk, H. R.) 73–108 (Academic, 1985).